IEEE Access
Multidisciplinary | Rapid Review | Open Access Journal

Received December 27, 2021, accepted January 14, 2022, date of publication January 18, 2022, date of current version January 27, 2022.

Digital Object Identifier 10.1109/ACCESS.2022.3144364

Performance of Cooperative Communication System With Multiple Reconfigurable Intelligent Surfaces Over Nakagami-*m* Fading Channels

VAN-DUC PHAN[1], BA CAO NGUYEN[2], TRAN MANH HOANG[2], TAN N. NGUYEN[3], (Member, IEEE), PHUONG T. TRAN[4], (Senior Member, IEEE), BUI VU MINH[5], AND MIROSLAV VOZNAK[6], (Senior Member, IEEE)

[1]Faculty of Automobile Technology, Van Lang University, Ho Chi Minh City 72900, Vietnam
[2]Faculty of Basic Techniques, Telecommunications University, Khanh Hoa 65000, Vietnam
[3]Communication and Signal Processing Research Group, Faculty of Electrical and Electronics Engineering, Ton Duc Thang University, Ho Chi Minh City 729000, Vietnam
[4]Wireless Communications Research Group, Faculty of Electrical and Electronics Engineering, Ton Duc Thang University, Ho Chi Minh City 729000, Vietnam
[5]Faculty of Mechanical, Electrical, Electronic & Automotive Engineering, Nguyen Tat Thanh University, Ho Chi Minh City 72900, Vietnam
[6]Faculty of Electrical Engineering and Computer Science, VSB—Technical University of Ostrava, 708 00 Ostrava, Czech Republic

Corresponding author: Tan N. Nguyen (nguyennhattan@tdtu.edu.vn)

This work was supported by the Ministry of Education, Youth and Sports of the Czech Republic, under Grant SP2021/25 and Grant e-INFRA CZ (ID: 90140).

ABSTRACT In this paper, the advantages of multiple reconfigurable intelligent surfaces (RISs) assisted wireless systems and direct link between two terminals are exploited by considering a cooperative communication system where reflecting links created by multiple RISs and the direct link are combined at the receiver. We mathematically analyze the performance of the cooperative multiple RISs - direct link (RIS-D) system over Nakagami-*m* fading channels by obtaining the symbol error probability (SEP) expression. In addition, the SEP of the single-input single-output (SISO) system without RISs (i.e., there is only direct link between two terminals) is also obtained for convenience in comparison the performance of the cooperative RIS-D and SISO systems. We demonstrate the correctness of the derived expressions via Monte-Carlo simulations. Numerical results show that the SEP of the cooperative RIS-D system significantly lower than that of the SISO system for a certain transmission power of the transmitter. Also, for a certain SEP target, the cooperative RIS-D system can greatly save energy consumption in comparison with the SISO system. Specifically, increasing the number of RISs or the number of reflecting elements (REs) in the RISs can remarkably reduce the SEP of the cooperative RIS-D system. On the other hand, the impacts of the system parameters such as the number of RISs, the number of REs, and the Nakagami-*m* fading channels are fully investigated to clearly indicate their influences on the SEP of the cooperative RIS-D system.

INDEX TERMS Cooperative communication, reconfigurable intelligent surface, method of moments, cumulative distribution function, symbol error probability.

I. INTRODUCTION

In the era of Internet of Things (IoT) devices and the fourth industrial revolution, high data transmission rate, high spectrum efficiency, high reliability, and low energy consumption are required for wireless communication systems, especially in the current and future cellular networks such as the fifth generation (5G) and beyond networks [1], [2]. To satisfy these requirements of the wireless communication systems, various solutions such as multiple antenna transmission, non-orthogonal multiple access, in-band full-duplex transmission, millimeter-wave, cooperative communication, and reconfigurable intelligent surface (RIS) have been proposed [3]–[6]. Among these techniques, RIS has been emerged as a promising candidate for the sixth generation (6G) and beyond systems [3], [7]. It is because that a RIS is a smart radio environment that can control the propagation of radio waves without energy source and receiver noise [8]. In addition, there are not converters (digital-to-analog and analog-to-digital) and amplifiers in the RIS, thus, the signal processing

The associate editor coordinating the review of this manuscript and approving it for publication was Farhana Jabeen Jabeen.

complexity when using RIS significantly reduces in comparison with using relay [5], [7], [8]. Furthermore, the RIS can provide full-duplex transmission and operate at any frequency. As the results, the usage of the RIS can provide high capacity, high quality of service, and reduce the energy consumption [8], [9].

Due to many advantages of the RIS, exploiting RIS for assisting wireless systems has been widely studied in the literature [5], [7], [8], [10]. It was shown that, a RIS-assisted two terminals wireless communication system can provide better performance than amplify-and-forward relay (AF) [5] or decode-and-forward (DF) relay [7] in terms of outage probability (OP) and spectral efficiency (SE). Specifically, via reflecting paths created by the RIS, the channel between two terminals in a wireless system is often characterized by Gamma distribution [5], [8]. Even small number of reflecting elements (REs) in the RIS, the performance in terms of the OP of a RIS-assisted wireless system is still higher than those of AF relay-assisted wireless system [5], [10]. However, in comparison with DF relay-assisted wireless system, the energy efficiency of the RIS-assisted wireless system is only higher in very high rates and larger number of REs [7]. On the other hand, the RIS assisted device-to-device communications and non-orthogonal multiple access systems have been investigated in the literature [11], [12].

Besides using one RIS, multiple reconfigurable intelligent surfaces (RISs) have been applied to assist wireless communication systems. Specifically, the combination of multiple reflecting paths created by multiple RISs in cooperative communications can significantly enhance the outage performance and ergodic capacity (EC) of the wireless systems [13]–[15]. It was also demonstrated that under the aid of the RISs, the propagation of radio waves can be controlled and optimized with a low complexity processing. Thus, the received signal power at the receiver can be maximized [15]. In addition, the distribution of the end-to-end channel created by multiple RISs and the direct link in the cooperative communications can be modeled by Gamma or LogNormal distributions [13]. Furthermore, expectation-maximization learning algorithm has been proposed for modeling the channel and improving the outage performance of the multiple RISs assisted wireless system [16]. Also, different channel models such as Rayleigh, Nakagami-*m*, and Rician fading channels have been considered for RISs assisted wireless communication systems [9], [17]–[19].

On the other hand, since the cooperative communication has many great advantages such as reducing costs in deployments, increasing the performance gain, and balancing quality of services [20], it had been used widely in the third and the fourth generation systems. It is because in the cooperative communication, the receiver can still receive the transmitter's signal through other channels if a channel is in deep fade. Consequently, the received signal power at the receiver in the case with cooperative communication is significantly enhanced in comparison with the case without cooperative communication. With many great advantages, the cooperative communication is still a main technique that can be used in 5G and 6G systems, especially when this technique is combined with other new techniques such as energy harvesting, full-duplex, and non-orthogonal multiple access [21].

As above discussions, the usage of one RIS or multiple RISs can significantly improve the coverage, capacity and quality of service of the wireless communication systems. Specifically, when multiple RISs are combined in the cooperative communications, the received signal power at the receiver greatly increases. In addition, all RISs can be located in different possible places, thus, in the case that the deep fading occurs in wireless propagation via one or two RISs, the signals are still propagated via other RISs to the receiver.[1] These signals can combine with the signal via direct link to remarkably increase the received signal power at the receiver. Therefore, the combination of multiple RISs and the direct link in the wireless communication systems is inevitable due to the fact that this combination can exploit the benefits of the direct link in traditional wireless systems and new recently technique (RISs). However, there is a lack of research on cooperative communication systems with multiple RISs and direct link between two terminals. Importantly, the advantages of using RIS for assisting wireless communication systems in terms of OP and EC have been analyzed in previous works [3], [5]–[7]. It was clearly indicated that the RIS-aided wireless communication systems can provide lower OP and higher EC than AF/DF relay-aided wireless communication systems [5]–[7]. Meanwhile, an other important factor of the wireless communication systems is symbol error probability (SEP) that was not given in previous works. In fact, SEP is a crucial factor due to the requirements of high capacity and low SEP for wireless communication systems. In the case that the SEP is high, the receivers cannot operate as expected. Motivated by this issue, in this paper, we consider a cooperative communication system, where multiple RISs are used and the direct link between two terminals is available. Specifically, Nakagami-*m* fading channels are considered for the cooperative system with multiple RISs and direct link (called as a cooperative RIS-D system). We mathematically derive the expression of SEP of the considered system. Then, we use the obtained expression to analyze the system performance in different scenarios. The main contributions of this paper can be summarized as follows:

- We consider a cooperative RIS-D system where the received signals at the receiver are combined of reflect paths via multiple RISs and direct path via direct link between two terminals. Specifically, N RISs equipped with L_n ($n = 1, 2, \ldots, N$) reflecting elements (REs) can locate in different locations for assisting two terminals

[1] As shown in [13], when the locations of the RISs are varied, the performance of the RIS-assisted wireless system will be changed. In addition, although the optimal locations of the RISs could not be derived due to the complexity of the OP and EC expressions, however, the locations of the RISs for improving the performance of wireless system can be figured out by using the obtained expressions. Specifically, the EC in the case that the RISs are located near either transmitter or receiver is higher than the EC in the case that the RISs are located further away from either transmitter or receiver [13].

in a wireless communication system. The reflect paths via multiple RISs are combined with a direct path via the direct link for improving the received signal power at the terminal. In addition, the Nakagami-m fading channels are applied in the considered cooperative RIS-D system.

- We obtain the closed-form expression of cumulative distribution function (CDF) of the end-to-end signal-to-noise ratio at the receiver by using method of moments. Then, we derive the closed-form expression of symbol error probability (SEP) of the considered cooperative RIS-D system over Nakagami-m fading channels. In addition, we also derive expression of SEP of the system without RISs, i.e., only the direct link between two terminals (called as single-input single-output (SISO) system). We demonstrate the correctness of the obtained expressions via Monte-Carlo simulations.
- We analyze the performance of the considered cooperative RIS-D system via various scenarios. Numerical results clearly show that the SEP performance of the considered cooperative RIS-D system are significantly improved in comparison with that of the SISO system. For a certain transmission power of the transmitter, the SEP of the cooperative RIS-D system is greatly lower than that of the SISO system. On the other hand, for a certain SEP target, the cooperative RIS-D system can greatly save the energy consumption in comparison with the SISO system. In addition, the usage of lager number of RISs, N, and lager number of REs, L_n, in the RISs can remarkably reduce the SEP of the considered cooperative RIS-D system. Furthermore, the impacts of the system parameters such as the number of RISs, the number of REs, and the Nakagami-m fading channels are also investigated to clearly indicate their influences on the SEP of the cooperative RIS-D system.

The rest of this paper is organized as follows. The system and signal models are presented in Section II, where the received signals at the receiver are clearly describe. Performance analysis of the cooperative RIS-D system is focused in Section III, where the closed-form expressions of SEP of the cooperative RIS-D and SISO systems are derived. Numerical results and discussions are provided in Section IV, where the impacts of the system parameters on the SEP of the considered system are detailedly evaluated. Finally, the conclusions of this paper are presented in Section V.

II. SYSTEM MODEL

Fig. 1 illustrates the system model of the cooperative system based on multiple RISs and direct link. Data are transmitted from S to D via S–R_n–D reflecting links and S–D direct link. S and D are half-duplex devices equipped with one antenna. Meanwhile, there are N distributed RISs, i.e., R_n, $n = 1, 2, \ldots, N$, where the nth RIS is equipped with L_n reflecting elements (REs). It is worth mentioning that in practical scenarios, the number of the REs in the RISs can be equal or different, i.e., $L_i = L_j$ or $L_i \neq L_j$ for $i \neq j$ and $i, j = 1, 2, \ldots, N$. In addition, the REs in the RISs can be adjusted by the communication oriented software [3].

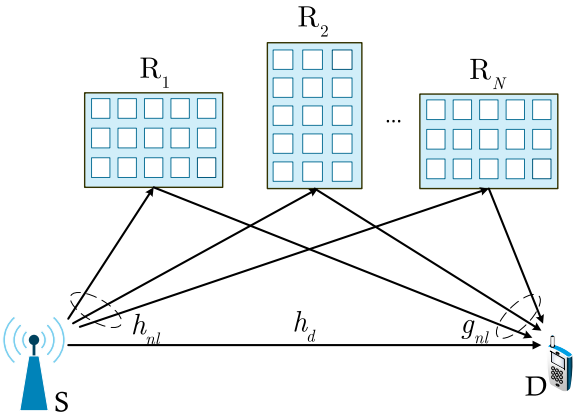

FIGURE 1. Illustrations of a cooperative RIS-D system with multiple RISs and direct link.

The received signals at D is given by

$$y_{\mathrm{D}} = \Big(h_d + \sum_{n=1}^{N}\sum_{l=1}^{L_n} h_{nl}k_{nl}g_{nl}\Big)x_{\mathrm{S}} + z_{\mathrm{D}}, \tag{1}$$

where x_{S} is the transmitted signal of S with the average transmission power of P_{S}; z_{D} is the Gaussian noise at D with zero mean and variance of σ_{D}^2, i.e., $z_{\mathrm{D}} \sim \mathcal{CN}(0, \sigma_{\mathrm{D}}^2)$; h_d is the fading channel coefficient of the S–D direct link; h_{nl} and g_{nl} are, respectively, the fading channel coefficients from S to lth reflecting element of the nth RIS and from lth reflecting element of the nth RIS to D; k_{nl} is the response of lth reflecting element of the nth RIS.

Since the fading channel coefficients are complex numbers, we can represent h_d, h_{nl}, and g_{nl} as $h_d = |h_d|e^{-j\phi_d}$, $h_{nl} = |h_{nl}|e^{-j\theta_{nl}}$, and $g_{nl} = |g_{nl}|e^{-j\psi_{nl}}$, where $|h_d|$, $|h_{nl}|$, and $|g_{nl}|$ are magnitudes and ϕ_d, θ_{nl}, and ψ_{nl} are phases of h_d, h_{nl}, and g_{nl}, respectively. On the other hand, as demonstrated in the literature such as [3], [7], [8], the RIS's features can be expressed via the diagonal matrix, i.e.,

$$\Theta = \mathrm{diag}(|k_{n1}|e^{j\varphi_{n1}}, \ldots, |k_{nl}|e^{j\varphi_{nl}}, \ldots, |k_{nL_n}|e^{j\varphi_{nL_n}}), \tag{2}$$

where $|k_{nl}| \in (0, 1)$ is the amplitude and φ_{nl} is the adjustable phase created by the lth reflecting element of the nth RIS. In other words, we have $k_{nl} = |k_{nl}|e^{j\varphi_{nl}}$.

In addition, since the Nakagami-m fading channels are considered in this paper, the instantaneous channel gains, i.e., $|h_d|^2$, $|h_{nl}|^2$, and $|g_{nl}|^2$ follow Gamma distributions. Mathematically, the probability density function (PDF, denoted by $f(x)$) and the cumulative distribution function (CDF, denoted by $F(x)$) of $|h|^2$ are given as

$$f_{|h|^2}(x) = \Big(\frac{m}{\Omega}\Big)^m \frac{x^{m-1}}{\Gamma(m)}\exp\Big(-\frac{mx}{\Omega}\Big), \quad x \geq 0, \tag{3}$$

$$F_{|h|^2}(x) = \frac{1}{\Gamma(m)}\gamma\Big(m, \frac{mx}{\Omega}\Big) = 1 - \exp\Big(-\frac{mx}{\Omega}\Big)\sum_{i=0}^{m-1}\frac{1}{i!}\Big(\frac{mx}{\Omega}\Big)^i, \quad x \geq 0, \tag{4}$$

where m and Ω are, respectively, the Nakagami parameter and the average channel gain of $|h|^2$; $\Gamma(.)$ and $\gamma(.,.)$ are, respectively, the gamma and the lower incomplete gamma functions. In the considered cooperative RIS-D system, the Nakagami parameters of the S–D channel, S–nth RIS channels, and nth RIS–D channels are, respectively, denoted by m_d, m_{h_n}, and m_{g_n}. Meanwhile, the average channel gains of the S–D channel, S–nth RIS channels, and nth RIS–D channels are, respectively, denoted by Ω_d, Ω_{h_n}, and Ω_{g_n}.

Now, the received signals at D is rewritten as

$$y_{\mathrm{D}} = \Big(|h_d|e^{-j\phi_d} + \sum_{n=1}^{N}\sum_{l=1}^{L_n}|h_{nl}|e^{-j\theta_{nl}} \times|k_{nl}|e^{j\varphi_{nl}}|g_{nl}|e^{-j\psi_{nl}}\Big)x_{\mathrm{S}} + z_{\mathrm{D}}. \quad (5)$$

Then, we reorganize (5) as

$$y_{\mathrm{D}} = e^{-j\phi_d}\Big(|h_d| + \sum_{n=1}^{N}\sum_{l=1}^{L_n}|h_{nl}| \times|k_{nl}||g_{nl}|e^{j(\varphi_{nl}-\theta_{nl}-\psi_{nl}+\phi_d)}\Big)x_{\mathrm{S}} + z_{\mathrm{D}}. \quad (6)$$

Let $\delta_{nl} = \varphi_{nl} - \theta_{nl} - \psi_{nl} + \phi_d$ be the phase error of the lth RE of the nth RIS, the received signals at D become

$$y_{\mathrm{D}} = e^{-j\phi_d}\Big(|h_d| + \sum_{n=1}^{N}\sum_{l=1}^{L_n}|h_{nl}||k_{nl}||g_{nl}|e^{j\delta_{nl}}\Big)x_{\mathrm{S}} + z_{\mathrm{D}}. \quad (7)$$

To enhance the received signal power at D, the adjustable phases of the RISs are adjusted. Mathematically, the ideal phase (denoted by φ_{nl}^*) of the lth RE of the nth RIS can be given as

$$\varphi_{nl}^* = \arg\max_{\varphi_{nl}} \gamma_{\mathrm{D}}, \quad \forall n, \quad \forall l, \quad (8)$$

where γ_{D} is the instantaneous signal-to-noise ratio (SNR) at D.

It was shown in recent reports that, the phase shifts of the REs depend on the diodes employed in the RISs [4], [22]. Thus, the phase shifts in practice may be not continuous due to the hardware limitations. As a result, the discrete phase shifts are more reasonable in the RIS-assisted wireless communication systems [4], [13]. Consequently, the number of phase shifts of the REs is constrained and limited by a phase shift resolution [4], [23]. Thus, the phase shift values are in the $[0, 2\pi)$ interval. Let b_n be the number of quantization bits and $\mathbb{R}_n \triangleq 2^{b_n}$ be the phase shift resolution of the nth RIS. Then, a phase shift value can be selected from the following set [4], [13]

$$\mathbb{S} = \left\{0, \frac{2\pi}{\mathbb{R}_n}, \frac{4\pi}{\mathbb{R}_n}, \ldots, \frac{2\pi(\mathbb{R}_n-1)}{\mathbb{R}_n}\right\}. \quad (9)$$

As presented in the literature, for a high phase shift resolution (i.e., $\mathbb{R}_n \gg 1$) and the perfect channel knowledges at the RISs, ideal phase shifts can be generated [4], [13], [17], [18]. Thus, the phase errors now are $\delta_{nl} = 0\ \forall n, \forall l$ [4], [13], [18]. Notice that the ideal phase shift assumption was widely used in the RIS-assisted wireless communication systems and it is inline with realistic implementations [4], [5], [13], [24]. In addition, this assumption has been extensively used for single-RIS-assisted wireless communication systems [3], [5], [7] and multi-RIS-assisted wireless communication systems [13], [17], [25]. It is also noted that in practice, the RIS-assisted wireless communication systems are generally implemented with discrete phase shifts. It is because that they are cost-effective and easy to achieve the ideal phase shifts. However, such implementation can reduce the performance of the RIS-assisted wireless communication systems [4].

Now, the ideal phase created by the lth RE of the nth RIS is calculated as

$$\varphi_{nl}^* = \theta_{nl} + \psi_{nl} - \phi_d. \quad (10)$$

Applying (10), (7) becomes

$$y_{\mathrm{D}} = e^{-j\phi_d}\Big(|h_d| + \sum_{n=1}^{N}\sum_{l=1}^{L_n}|h_{nl}||k_{nl}||g_{nl}|\Big)x_{\mathrm{S}} + z_{\mathrm{D}}. \quad (11)$$

Now, the instantaneous SNR at D is computed as

$$\gamma_{\mathrm{D}} = \frac{|e^{-j\phi_d}|^2\Big(|h_d| + \sum_{n=1}^{N}\sum_{l=1}^{L_n}|h_{nl}||k_{nl}||g_{nl}|\Big)^2 P_{\mathrm{S}}}{\sigma_{\mathrm{D}}^2}. \quad (12)$$

Due to the complex number properties, i.e., $|e^{-j\phi_d}|^2 = 1$, the instantaneous SNR expression at D now becomes

$$\gamma_{\mathrm{D}} = \frac{\Big(|h_d| + \sum_{n=1}^{N}\sum_{l=1}^{L_n}|h_{nl}||k_{nl}||g_{nl}|\Big)^2 P_{\mathrm{S}}}{\sigma_{\mathrm{D}}^2}. \quad (13)$$

III. PERFORMANCE ANALYSIS

In this section, we mathematically derive the SEP of the cooperative RIS-D system. Specifically, the SEP is expressed as

$$\mathrm{SEP} = a\mathbb{E}\{Q(\sqrt{b\gamma_{\mathrm{D}}})\} = \frac{a}{\sqrt{2\pi}}\int_0^{\infty} F\Big(\frac{t^2}{b}\Big)e^{-\frac{t^2}{2}}dt, \quad (14)$$

where (a, b) is a constant pair whose values are calculated from the certain modulation scheme, i.e., $(a, b) = (1, 2)$, $(a, b) = (2, 1)$, and $(a, b) = (3/2, 2/5)$ corresponding to binary phase-shift keying (BPSK), 4-quadrature amplitude modulation (4-QAM) or quadrature phase shift keying (QPSK), and 4-pulse amplitude modulation (4-PAM) [26]. The detail values of (a, b) for all modulation schemes are provided in Table 6.1 of [26]; $Q(z) \triangleq \frac{1}{\sqrt{2\pi}}\int_z^{\infty}\exp\left(-\frac{u^2}{2}\right)du$ is the Gaussian function; γ_{D} is SNR of the cooperative RIS-D system given in (13).

Let $x = \frac{t^2}{b}$ be a new variable, (14) now becomes

$$\mathrm{SEP} = \frac{a\sqrt{b}}{2\sqrt{2\pi}}\int_0^{\infty}\frac{F(x)}{\sqrt{x}}e^{-\frac{bx}{2}}dx. \quad (15)$$

From (15), we obtain the SEP of the cooperative RIS-D system in the following Theorem.

Theorem: The SEP of the cooperative RIS-D system over Nakagami-m fading channels is given as (16), as shown at the bottom of the page, where M is the Chebyshev parameter [27]; $\phi_i = \cos\left(\frac{(2i-1)\pi}{2M}\right)$; $\Gamma(.,.)$ is the upper incomplete gamma function; $\Xi_{\mathcal{X}}(1)$ and $\Xi_{\mathcal{X}}(2)$ are, respectively, the first and second moments of $\mathcal{X}$ (where $\mathcal{X} = |h_d| + \sum_{n=1}^{N}\sum_{l=1}^{L_n}|h_{nl}||k_{nl}||g_{nl}|$) calculated as

$$\Xi_{\mathcal{X}}(1) = \Xi_{h_0}(1) + \Xi_{\mathcal{Y}}(1), \tag{17}$$

$$\Xi_{\mathcal{X}}(2) = \Xi_{h_0}(2) + \Xi_{\mathcal{Y}}(2) + 2\Xi_{h_0}(1)\Xi_{\mathcal{Y}}(1), \tag{18}$$

$$\Xi_{\mathcal{Y}}(1) = \sum_{n=1}^{N}\sum_{l=1}^{L_n}\Xi_{\mathcal{T}_{nl}}(1), \tag{19}$$

$$\Xi_{\mathcal{Y}}(2) = \sum_{n=1}^{N}\Big[\sum_{l=1}^{L_n}\Xi_{\mathcal{T}_{nl}}(2) + 2\sum_{l=1}^{L_n}\Xi_{\mathcal{T}_{nl}}(1)\sum_{l'=l+1}^{L_n}\Xi_{\mathcal{T}_{nl'}}(1)\Big] + 2\sum_{n=1}^{N}\Big[\sum_{l=1}^{L_n}\Xi_{\mathcal{T}_{nl}}(1)\Big]\sum_{n'=n+1}^{N}\Big[\sum_{l=1}^{L_{n'}}\Xi_{\mathcal{T}_{n'l}}(1)\Big], \tag{20}$$

$$\Xi_{\mathcal{T}_{nl}}(p) = \lambda_{nl}^{-p}\frac{\Gamma(m_{h_n}+p/2)\Gamma(m_{g_n}+p/2)}{\Gamma(m_{h_n})\Gamma(m_{g_n})}, \tag{21}$$

$$\lambda_{nl} = \sqrt{\frac{m_{h_n}m_{g_n}}{|k_{nl}|^2\Omega_{h_n}\Omega_{g_n}}}, \tag{22}$$

$$\Xi_{h_0}(1) = \frac{\Gamma(m_d+1/2)}{\Gamma(m_d)}\sqrt{\frac{\Omega_d}{m_d}}, \tag{23}$$

$$\Xi_{h_0}(2) = \frac{\Gamma(m_d+1)}{\Gamma(m_d)}\frac{\Omega_d}{m_d} = \Omega_d. \tag{24}$$

Proof: To derive the SEP in (16), we firstly obtain the CDF of the considered cooperative RIS-D system, $F(x)$, to replace it into (15) for calculating. Mathematically, $F(x)$ is computed as

$$F(x) = \Pr\{\gamma_{\mathrm{D}} < x\}, \tag{25}$$

where Pr denotes the probability operator and γ_{D} is SNR of the considered cooperative RIS-D system.

Replacing γ_{D} in (13) into (25), we have

$$F(x) = \Pr\left\{\frac{\left(|h_d| + \sum_{n=1}^{N}\sum_{l=1}^{L_n}|h_{nl}||k_{nl}||g_{nl}|\right)^2 P_{\mathrm{S}}}{\sigma_{\mathrm{D}}^2} < x\right\}. \tag{26}$$

It is equivalent to

$$F(x) = \Pr\left\{\left(|h_d| + \sum_{n=1}^{N}\sum_{l=1}^{L_n}|h_{nl}||k_{nl}||g_{nl}|\right)^2 < \frac{\sigma_{\mathrm{D}}^2 x}{P_{\mathrm{S}}}\right\}. \tag{27}$$

For conveniences in calculating, we set $|h_d| = h_0$, $\mathcal{T}_{nl} = |h_{nl}||k_{nl}||g_{nl}|$, $\mathcal{Z}_n = \sum_{l=1}^{L_n}\mathcal{T}_{nl}$, $\mathcal{Y} = \sum_{n=1}^{N}\mathcal{Z}_n$, and $\mathcal{X} = |h_d| + \mathcal{Y} = h_0 + \mathcal{Y}$. Then, (27) becomes

$$F(x) = \Pr\left\{\mathcal{X}^2 < \frac{\sigma_{\mathrm{D}}^2 x}{P_{\mathrm{S}}}\right\} = F_{\mathcal{X}^2}\left(\frac{\sigma_{\mathrm{D}}^2 x}{P_{\mathrm{S}}}\right). \tag{28}$$

To derive the CDF from (28), we can firstly derive $F_{\mathcal{X}}(.)$ and then obtain $F_{\mathcal{X}^2}(.)$. Since h_0 and $\mathcal{Y}$ are independent, we can use the method of moments presented in [13] to obtain the CDF $F_{\mathcal{X}}(.)$.

On the other hand, since h_0 follows Nakagami distribution with Nakagami parameter m_d and average channel gain Ω_d, the pth moment of h_0, $\Xi_{h_0}(p) = \mathbb{E}\{h_0^p\}$, where $\mathbb{E}\{.\}$ denotes the expectation operator, is given as

$$\Xi_{h_0}(p) = \frac{\Gamma(m_d+p/2)}{\Gamma(m_d)}\left(\frac{m_d}{\Omega_d}\right)^{-p/2}. \tag{29}$$

From (29), we can easily obtain the first and the second moments of h_0 as in (23) and (24), respectively.

To obtain the pth moment of $\mathcal{T}_{nl} = |h_{nl}||k_{nl}||g_{nl}|$, we firstly derive the PDF of $\mathcal{T}_{nl}$, that is given as [13]

$$f_{\mathcal{T}_{nl}}(y) = \frac{1}{|k_{nl}|}\int_0^\infty \frac{1}{x}f_{|h_{nl}|}\left(\frac{y}{|k_{nl}|x}\right)f_{|g_{nl}|}(x)\,dx. \tag{30}$$

Similar to $|h_d|$, $|h_{nl}|$ and $|g_{nl}|$ follow Nakagami distributions with Nakagami parameters m_{h_n} and m_{g_n} and the average channel gains Ω_{h_n} and Ω_{g_n}, respectively, we have

$$f_{\mathcal{T}_{nl}}(y) = \frac{4}{\Gamma(m_{h_n})\Gamma(m_{g_n})}\left(\frac{m_{h_n}}{|k_{nl}|^2\Omega_{h_n}}\right)^{m_{h_n}}\left(\frac{m_{g_n}}{\Omega_{g_n}}\right)^{m_{gn}} \times y^{2m_{h_n}-1}\int_0^\infty x^{2m_{g_n}-2m_{h_n}-1} \times \exp\left(-\frac{y^2 m_{h_n}}{|k_{nl}|^2\Omega_{h_n}x^2} - \frac{m_{g_n}x^2}{\Omega_{g_n}}\right)dx. \tag{31}$$

Applying [28, Eq. (3.478.4)], (31) becomes

$$f_{\mathcal{T}_{nl}}(y) = \frac{4\lambda_{nl}^{m_{h_n}+m_{g_n}}}{\Gamma(m_{h_n})\Gamma(m_{g_n})}y^{m_{h_n}+m_{g_n}-1}\mathcal{K}_{m_{g_n}-m_{h_n}}(2\lambda_{nl}y), \tag{32}$$

where λ_{nl} is given in (22) and $\mathcal{K}_{m_{g_n}-m_{h_n}}(.)$ is the $m_{g_n}-m_{h_n}$ order modified Bessel function of the second kind [28].

$$\mathrm{SEP} = \frac{a\sqrt{b}}{2\sqrt{2\pi}}\left[\sqrt{\frac{2\pi}{b}} - \frac{\pi}{M\Gamma\left(\frac{[\Xi_{\mathcal{X}}(1)]^2}{\Xi_{\mathcal{X}}(2)-[\Xi_{\mathcal{X}}(1)]^2}\right)}\sum_{i=1}^{M}\sqrt{\frac{1-\phi_i^2}{2b[\ln 2 - \ln(1+\phi_i)]}} \times \Gamma\left(\frac{[\Xi_{\mathcal{X}}(1)]^2}{\Xi_{\mathcal{X}}(2)-[\Xi_{\mathcal{X}}(1)]^2}, \frac{\Xi_{\mathcal{X}}(1)}{\Xi_{\mathcal{X}}(2)-[\Xi_{\mathcal{X}}(1)]^2}\sqrt{\frac{2\sigma_{\mathrm{D}}^2[\ln 2 - \ln(1+\phi_i)]}{bP_{\mathrm{S}}}}\right)\right], \tag{16}$$

Consequently, the pth moment of $\mathcal{T}_{nl}$ is expressed as

$$\Xi_{\mathcal{T}_{nl}}(p) = \mathbb{E}\{\mathcal{T}_{nl}^p\} = \int_0^\infty y^p f_{\mathcal{T}_{nl}}(y)dy. \tag{33}$$

Applying [28, Eq. (6.561.16)], $\Xi_{\mathcal{T}_{nl}}(p)$ from (33) is given in (21). Then, based on the pth moment of $\mathcal{T}_{nl}$, we can represent $\mathcal{T}_{nl}$ via Gamma distribution such as (3) and (4) [13]. Mathematically, the CDF of $\mathcal{T}_{nl}$ can be expressed as

$$F_{\mathcal{T}_{nl}}(x) \approx \frac{1}{\Gamma\left(\frac{[\Xi_{\mathcal{T}_{nl}}(1)]^2}{\Xi_{\mathcal{T}_{nl}}(2)-[\Xi_{\mathcal{T}_{nl}}(1)]^2}\right)} \times\gamma\left(\frac{[\Xi_{\mathcal{T}_{nl}}(1)]^2}{\Xi_{\mathcal{T}_{nl}}(2)-[\Xi_{\mathcal{T}_{nl}}(1)]^2}, \frac{\Xi_{\mathcal{T}_{nl}}(1)x}{\Xi_{\mathcal{T}_{nl}}(2)-[\Xi_{\mathcal{T}_{nl}}(1)]^2}\right). \tag{34}$$

Since $\mathcal{Z}_n = \sum_{l=1}^{L_n} \mathcal{T}_{nl}$, the approximate CDF of $\mathcal{Z}_n$ is expressed as [3]

$$F_{\mathcal{Z}_n}(x) \approx \frac{1}{\Gamma\left(\frac{L_n[\Xi_{\mathcal{T}_{nl}}(1)]^2}{\Xi_{\mathcal{T}_{nl}}(2)-[\Xi_{\mathcal{T}_{nl}}(1)]^2}\right)} \times\gamma\left(\frac{L_n[\Xi_{\mathcal{T}_{nl}}(1)]^2}{\Xi_{\mathcal{T}_{nl}}(2)-[\Xi_{\mathcal{T}_{nl}}(1)]^2}, \frac{\Xi_{\mathcal{T}_{nl}}(1)x}{\Xi_{\mathcal{T}_{nl}}(2)-[\Xi_{\mathcal{T}_{nl}}(1)]^2}\right). \tag{35}$$

It is worth noticing that, although the Gamma approximations are used in (34) and (35), the differences between the approximate results and the exact results are very small. Consequently, the analysis results nearly perfectly match with the simulation results in the RIS-aided wireless communication systems using Gamma approximations [3], [5], [9], [12], [13].

Then, using multinomial expression [29], the pth moment of $\mathcal{Z}_n$ can be computed as

$$\begin{aligned}\Xi_{\mathcal{Z}_n}(p) &= \mathbb{E}\{\mathcal{Z}_n^p\} \\ &= \sum_{p_1=0}^{p}\sum_{p_2=0}^{p_1}\cdots\sum_{p_{L_n-1}=0}^{p_{L_n-2}}\binom{p}{p_1}\binom{p_1}{p_2}\cdots\binom{p_{L_n-2}}{p_{L_n-1}} \\ &\quad\times\Xi_{\mathcal{T}_{n1}}(p-p_1)\Xi_{\mathcal{T}_{n2}}(p_1-p_2)\cdots\Xi_{\mathcal{T}_{nL_n}}(p_{L_n-1}),\end{aligned} \tag{36}$$

where $\binom{n}{k} = \frac{n!}{k!(n-k)!}$.

Similar to $\mathcal{Z}_n$, the pth moment of $\mathcal{Y}$ can be obtained as

$$\begin{aligned}\Xi_{\mathcal{Y}}(p) &= \mathbb{E}\{\mathcal{Y}^p\} \\ &= \sum_{p_1=0}^{p}\sum_{p_2=0}^{p_1}\cdots\sum_{p_{N-1}=0}^{p_{N-2}}\binom{p}{p_1}\binom{p_1}{p_2}\cdots\binom{p_{N-2}}{p_{N-1}} \\ &\quad\times\Xi_{\mathcal{Z}_1}(p-p_1)\Xi_{\mathcal{Z}_2}(p_1-p_2)\cdots\Xi_{\mathcal{Z}_N}(p_{N-1}).\end{aligned} \tag{37}$$

Combining of (21), (36), and (37), we can obtain the first and the second moments of $\mathcal{Y}$ as in (19) and (20), respectively.

On the other hand, due to the independence of h_0 and $\mathcal{Y}$, we can derive the pth moment of $\mathcal{X} = h_0 + \mathcal{Y}$ as

$$\begin{aligned}\Xi_{\mathcal{X}}(p) &= \mathbb{E}\{(h_0+\mathcal{Y})^p\} = \mathbb{E}\left\{\sum_{l=0}^{p}\binom{p}{l}h_0^l\mathcal{Y}^{p-l}\right\} \\ &= \sum_{l=0}^{p}\binom{p}{l}\Xi_{h_0}(l)\Xi_{\mathcal{Y}}(p-l).\end{aligned} \tag{38}$$

From (38), we can obtain the first and the second moments of $\mathcal{X}$ in (17) and (18), respectively.

Now, the CDF of $\mathcal{X}$ can be given as

$$F_{\mathcal{X}}(x) = \frac{1}{\Gamma\left(\frac{[\Xi_{\mathcal{X}}(1)]^2}{\Xi_{\mathcal{X}}(2)-[\Xi_{\mathcal{X}}(1)]^2}\right)} \times\gamma\left(\frac{[\Xi_{\mathcal{X}}(1)]^2}{\Xi_{\mathcal{X}}(2)-[\Xi_{\mathcal{X}}(1)]^2}, \frac{\Xi_{\mathcal{X}}(1)x}{\Xi_{\mathcal{X}}(2)-[\Xi_{\mathcal{X}}(1)]^2}\right). \tag{39}$$

Consequently, we have

$$\begin{aligned}F_{\mathcal{X}^2}(x) &= \Pr\{\mathcal{X}^2 < x\} = \Pr\{\mathcal{X} < \sqrt{x}\} \\ &= \frac{1}{\Gamma\left(\frac{[\Xi_{\mathcal{X}}(1)]^2}{\Xi_{\mathcal{X}}(2)-[\Xi_{\mathcal{X}}(1)]^2}\right)} \times\gamma\left(\frac{[\Xi_{\mathcal{X}}(1)]^2}{\Xi_{\mathcal{X}}(2)-[\Xi_{\mathcal{X}}(1)]^2}, \frac{\Xi_{\mathcal{X}}(1)\sqrt{x}}{\Xi_{\mathcal{X}}(2)-[\Xi_{\mathcal{X}}(1)]^2}\right).\end{aligned} \tag{40}$$

Therefore, the CDF of γ_{D} is given as

$$\begin{aligned}F_{\mathcal{X}^2}\left(\frac{\sigma_{\mathrm{D}}^2 x}{P_{\mathrm{S}}}\right) &= \frac{1}{\Gamma\left(\frac{[\Xi_{\mathcal{X}}(1)]^2}{\Xi_{\mathcal{X}}(2)-[\Xi_{\mathcal{X}}(1)]^2}\right)} \\ &\quad\times\gamma\left(\frac{[\Xi_{\mathcal{X}}(1)]^2}{\Xi_{\mathcal{X}}(2)-[\Xi_{\mathcal{X}}(1)]^2}, \right. \\ &\qquad\left.\frac{\Xi_{\mathcal{X}}(1)}{\Xi_{\mathcal{X}}(2)-[\Xi_{\mathcal{X}}(1)]^2}\sqrt{\frac{\sigma_{\mathrm{D}}^2 x}{P_{\mathrm{S}}}}\right).\end{aligned} \tag{41}$$

Since $\Gamma(a,x)+\gamma(a,x) = \Gamma(a)$, (41) can be rewritten as

$$\begin{aligned}F_{\mathcal{X}^2}\left(\frac{\sigma_{\mathrm{D}}^2 x}{P_{\mathrm{S}}}\right) &= 1 - \frac{1}{\Gamma\left(\frac{[\Xi_{\mathcal{X}}(1)]^2}{\Xi_{\mathcal{X}}(2)-[\Xi_{\mathcal{X}}(1)]^2}\right)} \\ &\quad\times\Gamma\left(\frac{[\Xi_{\mathcal{X}}(1)]^2}{\Xi_{\mathcal{X}}(2)-[\Xi_{\mathcal{X}}(1)]^2}, \right. \\ &\qquad\left.\frac{\Xi_{\mathcal{X}}(1)}{\Xi_{\mathcal{X}}(2)-[\Xi_{\mathcal{X}}(1)]^2}\sqrt{\frac{\sigma_{\mathrm{D}}^2 x}{P_{\mathrm{S}}}}\right).\end{aligned} \tag{42}$$

Replacing (42) into (15), the SEP is now calculated as (43), as shown at the bottom of the next page.

First, using [28, Eq. (3.361.2)] to solve the first integral in (43), i.e.,

$$\int_0^\infty \frac{e^{-\frac{bx}{2}}}{\sqrt{x}}dx = \sqrt{\frac{2\pi}{b}}. \tag{44}$$

Then, setting $t = e^{-\frac{bx}{2}}$, the second integral in (43) can be expressed as (45), as shown at the bottom of the next page. Now, applying [27, Eq. (25.4.30)], we have (46), as shown at the bottom of the next page. Replacing (44) and (46) into (43), we obtain the SEP of the considered system as in the Theorem. This ends the proof.

It is worth pointing that the SEP expression given in (16) includes some special functions such as gamma and incomplete gamma, approximating these functions in the extreme conditions can cause a big gap between theoretical and simulated results due to the properties of this expression. Therefore, in this paper, the asymptotic form of the SEP of the cooperative RIS-D system was not provided.

On the other hand, after obtaining the SEP of the considered system, we can directly derive the diversity order from the SEP. In this paper, the SEP expression given in (16) is very complex, thus, it is too difficult to calculate the diversity order of the system from this expression. However, based on the previous works where multiple RISs are used to assist wireless communication systems [13], [17], the diversity order of the considered cooperative RIS-D system can also be derived. In particular, the work in [17] derived the OP and EC expressions of the multiple RISs-assisted wireless communication system without direct link between two terminals. Then, the authors obtained the diversity order of the system via OP expression as NL. In this paper, since the direct link between two terminal is available, the diversity order of the considered cooperative RIS-D system can be obtained as $1 + NL$.

It is also noted that in the case without the RISs, i.e., only direct link from S to D (SISO system), based on the CDF given in (4), the SEP in this the case (denoted by SEP_d) is given as

$$\mathrm{SEP}_d = \frac{a\sqrt{b}}{2\sqrt{2\pi}}\left[\sqrt{\frac{2\pi}{b}} - \sum_{i=0}^{m_d-1}\frac{1}{i!}\left(\frac{m_d\sigma_{\mathrm{D}}^2}{\Omega_d P_{\mathrm{S}}}\right)^i \Gamma\left(i+\frac{1}{2}\right) \times \frac{1}{\left(\frac{b}{2}+\frac{m_d\sigma_{\mathrm{D}}^2}{\Omega_d P_{\mathrm{S}}}\right)^{i+\frac{1}{2}}}\right]. \quad (47)$$

IV. NUMERICAL RESULTS AND DISCUSSIONS

In this section, we use the derived expressions of SEP in previous section to investigate the performance of the considered cooperative RSI-D system. Monte-Carlo simulations are also provided to demonstrate the correctness of the obtained expressions by using 10^6 channel realizations. Specifically, similar to the work in [7], the bandwidth is set as BW $=$ 10 MHz corresponding to the noise power $\sigma_{\mathrm{D}}^2 = -94$ dBm calculated from $\sigma_{\mathrm{D}}^2 = N_0 + 10\log(\mathrm{BW}) + \mathrm{NF}$ [dBm], where N_0 and NF are, respectively, the thermal noise power density [dBm/Hz] and the noise figure [dBm], they are set as $N_0 = -174$ and $\mathrm{NF} = 10$. In addition, the path loss models are aggregated in the average channel gains of the Nakagami-m fading channels [7], [9], i.e., $\Omega_d = G_{\mathrm{S}} + G_{\mathrm{D}} - 22.7 - 26\log(f_c) - 36.7\log(d_{\mathrm{SD}}/d_0)$, $\Omega_{h_n} = G_{\mathrm{S}} + G_{\mathrm{R}_n} - 22.7 - 26\log(f_c) - 36.7\log(d_{\mathrm{SR}_n}/d_0)$, and

$$\begin{aligned}\mathrm{SEP} &= \frac{a\sqrt{b}}{2\sqrt{2\pi}}\int_0^\infty \frac{e^{-\frac{bx}{2}}}{\sqrt{x}}\left[1 - \frac{1}{\Gamma\left(\frac{[\Xi_{\mathcal{X}}(1)]^2}{\Xi_{\mathcal{X}}(2)-[\Xi_{\mathcal{X}}(1)]^2}\right)}\Gamma\left(\frac{[\Xi_{\mathcal{X}}(1)]^2}{\Xi_{\mathcal{X}}(2)-[\Xi_{\mathcal{X}}(1)]^2}, \frac{\Xi_{\mathcal{X}}(1)}{\Xi_{\mathcal{X}}(2)-[\Xi_{\mathcal{X}}(1)]^2}\sqrt{\frac{\sigma_{\mathrm{D}}^2 x}{P_{\mathrm{S}}}}\right)\right]dx \\ &= \frac{a\sqrt{b}}{2\sqrt{2\pi}}\left[\int_0^\infty \frac{e^{-\frac{bx}{2}}}{\sqrt{x}}dx - \frac{1}{\Gamma\left(\frac{[\Xi_{\mathcal{X}}(1)]^2}{\Xi_{\mathcal{X}}(2)-[\Xi_{\mathcal{X}}(1)]^2}\right)}\int_0^\infty \frac{e^{-\frac{bx}{2}}}{\sqrt{x}}\Gamma\left(\frac{[\Xi_{\mathcal{X}}(1)]^2}{\Xi_{\mathcal{X}}(2)-[\Xi_{\mathcal{X}}(1)]^2}, \frac{\Xi_{\mathcal{X}}(1)}{\Xi_{\mathcal{X}}(2)-[\Xi_{\mathcal{X}}(1)]^2}\sqrt{\frac{\sigma_{\mathrm{D}}^2 x}{P_{\mathrm{S}}}}\right)dx\right]. \quad (43)\end{aligned}$$

$$\begin{aligned}&\int_0^\infty \frac{e^{-\frac{bx}{2}}}{\sqrt{x}}\Gamma\left(\frac{[\Xi_{\mathcal{X}}(1)]^2}{\Xi_{\mathcal{X}}(2)-[\Xi_{\mathcal{X}}(1)]^2}, \frac{\Xi_{\mathcal{X}}(1)}{\Xi_{\mathcal{X}}(2)-[\Xi_{\mathcal{X}}(1)]^2}\sqrt{\frac{\sigma_{\mathrm{D}}^2 x}{P_{\mathrm{S}}}}\right)dx \\ &\quad= -\int_1^0 \frac{t}{\sqrt{\frac{2}{b}\ln\frac{1}{t}}}\Gamma\left(\frac{[\Xi_{\mathcal{X}}(1)]^2}{\Xi_{\mathcal{X}}(2)-[\Xi_{\mathcal{X}}(1)]^2}, \frac{\Xi_{\mathcal{X}}(1)}{\Xi_{\mathcal{X}}(2)-[\Xi_{\mathcal{X}}(1)]^2}\sqrt{\frac{2\sigma_{\mathrm{D}}^2}{bP_{\mathrm{S}}}\ln\frac{1}{t}}\right)\left(\frac{-2}{b}\right)\frac{dt}{t} \\ &\quad= 2\int_0^1 \frac{1}{\sqrt{2b\ln\frac{1}{t}}}\Gamma\left(\frac{[\Xi_{\mathcal{X}}(1)]^2}{\Xi_{\mathcal{X}}(2)-[\Xi_{\mathcal{X}}(1)]^2}, \frac{\Xi_{\mathcal{X}}(1)}{\Xi_{\mathcal{X}}(2)-[\Xi_{\mathcal{X}}(1)]^2}\sqrt{\frac{2\sigma_{\mathrm{D}}^2}{bP_{\mathrm{S}}}\ln\frac{1}{t}}\right)dt. \quad (45)\end{aligned}$$

$$\begin{aligned}&2\int_0^1 \frac{1}{\sqrt{2b\ln\frac{1}{t}}}\Gamma\left(\frac{[\Xi_{\mathcal{X}}(1)]^2}{\Xi_{\mathcal{X}}(2)-[\Xi_{\mathcal{X}}(1)]^2}, \frac{\Xi_{\mathcal{X}}(1)}{\Xi_{\mathcal{X}}(2)-[\Xi_{\mathcal{X}}(1)]^2}\sqrt{\frac{2\sigma_{\mathrm{D}}^2}{bP_{\mathrm{S}}}\ln\frac{1}{t}}\right)dt \\ &\quad= \frac{\pi}{M}\sum_{i=1}^{M}\sqrt{\frac{1-\phi_i^2}{2b[\ln 2 - \ln(1+\phi_i)]}}\Gamma\left(\frac{[\Xi_{\mathcal{X}}(1)]^2}{\Xi_{\mathcal{X}}(2)-[\Xi_{\mathcal{X}}(1)]^2}, \frac{\Xi_{\mathcal{X}}(1)}{\Xi_{\mathcal{X}}(2)-[\Xi_{\mathcal{X}}(1)]^2}\sqrt{\frac{2\sigma_{\mathrm{D}}^2[\ln 2 - \ln(1+\phi_i)]}{bP_{\mathrm{S}}}}\right). \quad (46)\end{aligned}$$

TABLE 1. Simulation parameters.

Notation	Description	Fixed value	Varying range
P_{S}	Transmission power of S	none	$-5 \sim 25$ dBm
N	Number of RISs	4	1, 3, 5, 7, 9, 11
L	Number of REs	25	10, 15, 20, 25, 30, 35, 40
(a, b)	A pair of the modulation types	$(2, 1)$	$(1, 2)$, $(3/2, 2/5)$
$\lvert k_{nl}\rvert$	Amplitude of lth RE of the nth RIS	1	none
m_d, m_{h_n}, m_{g_n}	Nakagami parameters	2	1, 3
d_{SD}	Distance between S and D	100 m	none
f_c	Carrier frequency	3 GHz	none
$G_{\mathrm{S}}, G_{\mathrm{R}_n}, G_{\mathrm{D}}$	Antenna gains	5 dB	0 dB
$\sum_n^N L_n$	Total REs	125	20, 60, 100, 140, 180, 220
BW	Bandwidth	10 MHz	none
N_0	Thermal noise power density	-174 dBm/Hz	none
NF	Noise figure	10 dBm	none
$x_{\mathrm{R}_n}, y_{\mathrm{R}_n}$	Location of RISs	$x_{\mathrm{R}_n} = 50$, $y_{\mathrm{R}_n} = 5$	$x_{\mathrm{R}_n} \in [10, 90]$, $y_{\mathrm{R}_n} \in [1, 9]$

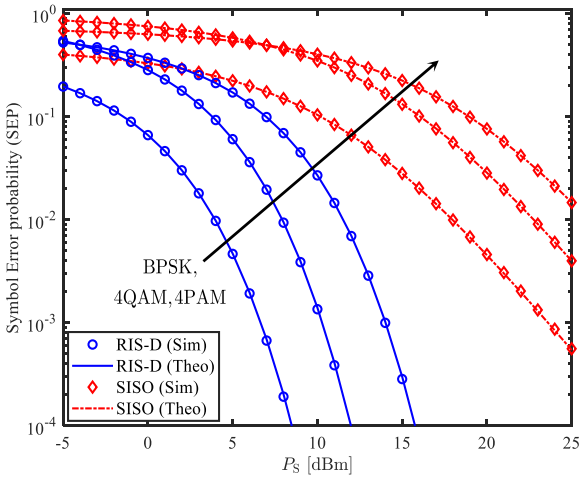

FIGURE 2. The SEP of the considered cooperative RIS-D system versus the average transmission power for different modulation schemes, i.e., BPSK, 4QAM, and 4 PAM; $N = 5$ RISs, $L_n = 25$ REs, $m_d = m_{h_n} = m_{g_n} = 2$.

$\Omega_{g_n} = G_{\mathrm{R}_n} + G_{\mathrm{D}} - 22.7 - 26\log(f_c) - 36.7\log(d_{\mathrm{R}_n\mathrm{D}}/d_0)$ $(n = 1, 2, \ldots, N)$, where G_{S}, G_{R_n}, and G_{D} are, respectively the antenna gains at S, R_n, and D. We set $G_{\mathrm{S}} = 5$ dB, $G_{\mathrm{R}_n} = 5$ dB, and $G_{\mathrm{D}} = 0$ dB; f_c is the carrier frequency, which is chosen as $f_c = 3$ GHz; d_0 is the reference distance, which is normalized as $d_0 = 1$ meter; d_{SD} is the distance between S and D which is set as $d_{\mathrm{SD}} = 100$ meters; d_{SR_n} and $d_{\mathrm{R}_n\mathrm{D}}$ are, respectively the distances from S to R_n and from R_n to D, that are varied in different scenarios. The RISs are located between S and D, where the certain locations of the RISs is presented via coordinate axis, i.e., x_{R_n} and y_{R_n}. For clarity, the simulation parameters used in this section are provided in Tab. 1.

Fig. 2 illustrates the SEP of the considered cooperative RIS-D system versus the average transmission power in comparison with the SEP of the SISO system (without RISs) for

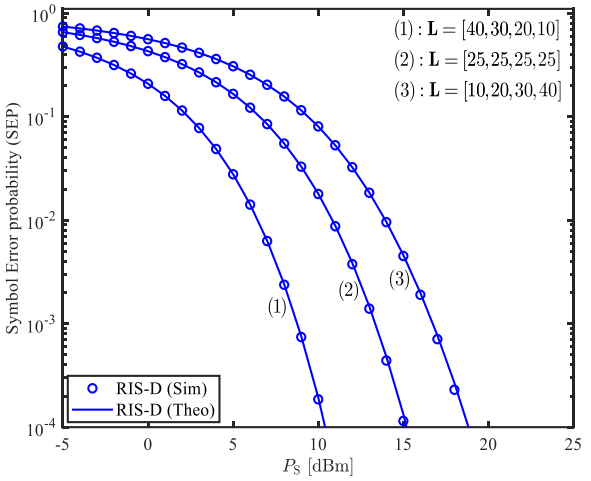

FIGURE 3. The SEP the considered cooperative RIS-D system for different number of REs in the RISs using 4QAM; $N = 4$; $\mathbf{L} = [40, 30, 20, 10]$, $\mathbf{L} = [25, 25, 25, 25]$, and $\mathbf{L} = [10, 20, 30, 40]$; $m_d = m_{h_n} = m_{g_n} = 2$; $(x_{\mathbf{R}_n}, y_{\mathbf{R}_n}) = (7, 2), (13, 6), (41, 8), (75, 4)$.

different modulation schemes, i.e., BPSK $((a, b) = (1, 2))$, 4QAM $((a, b) = (2, 1))$, and 4 PAM $((a, b) = (3/2, 2/5))$. We use $N = 5$ RISs and $L_n = 25$ REs $(n = 1, 2, \ldots, 5)$. The Nakagami parameters are set as $m_d = m_{h_n} = m_{g_n} = 2$. The theory curves are obtained by using (16) and (47) for the cooperative RIS-D and SISO systems, respectively. Meanwhile, the marker symbols denote Monte-Carlo simulation results. As observed from Fig. 2 that, under the assistance of the RISs, the performance of the wireless system can significantly improve in comparison with the case without RISs. It is because the SEPs of the cooperative RIS-D system are greatly lower than those of the SISO system. Specifically, the SEPs of the cooperative RIS-D system can reach 10^{-4} when $P_{\mathrm{S}} = 8$, 12, and 16 dBm corresponding to BPSK, 4QAM, and 4PAM. Meanwhile, even high transmission power of S, i.e., $P_{\mathrm{S}} = 25$ dBm, the SEPs of the SISO system only reach 5×10^{-4}, 4×10^{-3}, and 1.5×10^{-2} corresponding to BPSK, 4QAM, and 4PAM. As the results, we can use multiple RISs combing with the direct link in the cooperative communications for significantly enhancing the performance of the wireless systems.

Fig. 3 considers the SEP of the cooperative RIS-D system for different number of REs in the RISs. In the investigated scenario, we set $N = 4$ and the total REs in all the RISs is 100 REs. In addition, vector $\mathbf{L}$ is presented as $\mathbf{L} = [L_1, L_2, L_3, L_4]$. Furthermore, the coordinates of the RISs are set as $(x_{\mathrm{R}_n}, y_{\mathrm{R}_n}) = (7, 2), (13, 6), (41, 8), (75, 4)$. For these settings, the 1st RIS (L_1) is located nearest from S while the 4th RIS (L_4) is located furthest from S. As can be seen from Fig. 3, the case that $\mathbf{L} = [40, 30, 20, 10]$ is the best case and the case that $\mathbf{L} = [10, 20, 30, 40]$ is the worst case among three considered cases. As a result, the RIS located nearly from S can reflect signals better than the RIS located further from S. It is because the SEP in the case one ($\mathbf{L} = [40, 30, 20, 10]$) is significantly lower than the SEP in the case three ($\mathbf{L} = [10, 20, 30, 40]$). In particular, when SEP

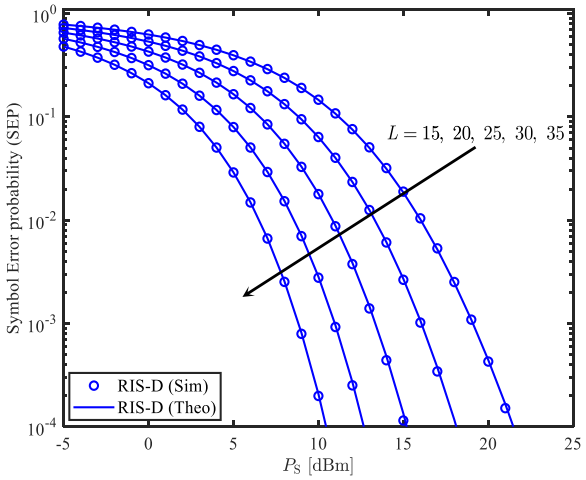

FIGURE 4. The impacts of the total number of REs on the SEP of the considered cooperative RIS-D system using 4QAM; $N = 4$; $L_1 = L_2 = L_3 = L_4 = L = 15, 20, 25, 30, 35$; $m_d = m_{h_n} = m_{g_n} = 2$.

target is 10^{-4}, the first case ($\mathbf{L} = [40, 30, 20, 10]$) only needs $P_S \approx 11$ dBm while the third case ($\mathbf{L} = [10, 20, 30, 40]$) needs $P_S \approx 18$ dBm. Therefore, we can locate the RIS with larger REs nearly the transmitter for improving the performance of the considered cooperative RIS-D system.[2]

Fig. 4 investigates the impacts of the total number of REs in the RISs on the SEP of the considered cooperative RIS-D system, where $L_1 = L_2 = L_3 = L_4 = L = 15, 20, 25, 30$, and 35 REs. It is obvious from Fig. 4 that increasing the number of REs in the RISs can significantly improve the SEP performance of the cooperative RIS-D system. In particular, the transmission power of S is approximate 10.5, 12.5, 15, 18, and 21.5 dBm corresponding to $L = 15, 20, 25, 30$, and 35 REs to obtain SEP $= 10^{-4}$. In other words, when the total number of REs in all RISs is plus 20 REs, i.e., from $L = 15$ ($4 \times 15 = 60$ REs) to $L = 20$ ($4 \times 20 = 80$ REs), or from $L = 20$ to $L = 25$, or from $L = 25$ to $L = 30$, the transmission power of S can be approximately reduced from 2 to 3 dBm for a SEP target of 10^{-4}. As the results, for a certain SEP target, the usage of multiple RISs with larger total number of REs can greatly save the energy consumption because the transmission power of source is significantly reduced.

In Fig. 5, we fix the total number of REs in each RIS, i.e., $L_n = 20$ REs for all $n \in N$ while the number of RISs is varied, i.e., $N = 1, 3, 5, 7, 9, 11$. Similar to the SEP in Fig. 4, the SEP in Fig. 5 is significantly reduced when N increases. Specifically, when the system requirement is SEP $= 10^{-4}$, increasing N from 1 to 3 can reduce the transmission power of the source from 21 dBm to 18 dBm. In other words, the energy consumption is reduced 3 dBm when N increases

[2]It is worth noticing that when all the RISs are placed at equal distance from the source and destination and the total REs in all RISs is constant, the SEPs in the case of the numbers of REs in the RISs are different can be lower than SEP in the case of the numbers of REs in the RISs are similar. This feature also occurs for the OP performance of the RISs-aided wireless systems [13], [17], [30].

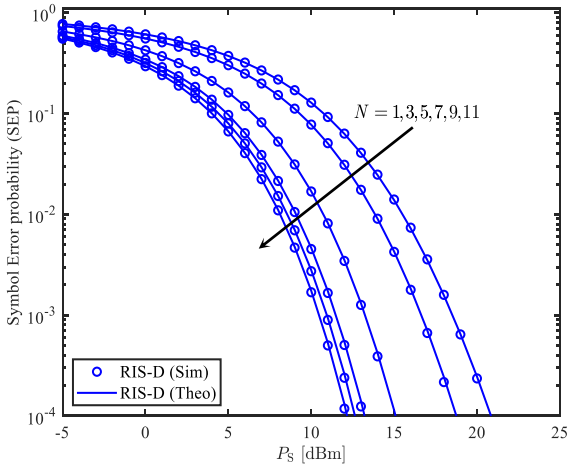

FIGURE 5. The SEP of the considered cooperative RIS-D system using 4QAM for $N = 1, 3, 5, 7, 9, 11$; $L_n = 20$ ($n = 1, 2, \ldots, N$); $m_d = m_{h_n} = m_{g_n} = 2$.

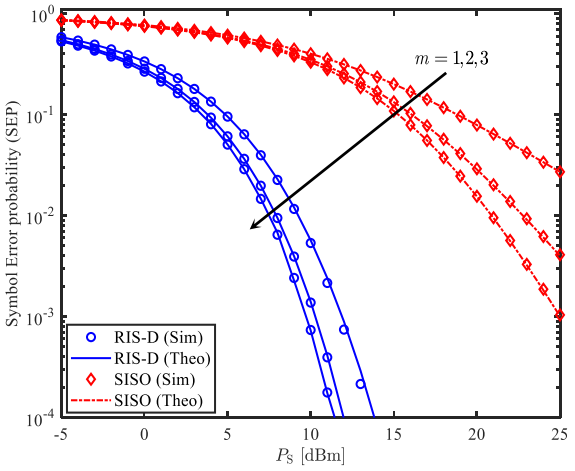

FIGURE 6. The impact of the Nakagami parameter m on the SEP of the considered RIS-D system for $N = 5$, $L_n = 25$, using 4QAM.

from 1 to 3. On the other hand, when the transmission power of the source is $P_S = 18$ dBm, the SEPs are 1.6×10^{-3} and 2.4×10^{-4} for $N = 1$ and $N = 3$, respectively. As a result, the SEP is approximately reduced 6.7 times when N increases from 1 to 3 for $P_S = 18$ dBm. When N continuously increases, i.e., $N = 5, 7, 9$, and 11, the SEP continuously reduces. However, the reduction for larger range of N is slower in comparison with the reduction for small N. For example, the SEP reduction when N increases from 7 to 9 or from 9 to 11 is lower than that when N increases from 1 to 3 or from 3 to 5. Therefore, depending on the certain requirements of the wireless system in practice, we can choose a suitable value of N for improving the performance and saving the energy of the cooperative RIS-D system.

Fig. 6 evaluates the impact of the Nakagami parameter m on the SEP of the considered RIS-D system for $N = 5$ and $L_n = 25$ REs. It is worth noticing that in the case of $m = 1$, the Nakagami-m fading channels become the Rayleigh fading channels. As can be seen from Fig. 6, increasing m can significantly enhance the SEP performance of the cooperative

RIS-D and SISO systems, especially in high transmission power regime. Particularly, the differences between the SEPs in the cases of $m = 1, 2$, and 3 of the SISO system for $P_S < 15$ dBm are very small. However, they are remarkable for $P_S > 15$ dBm. Specifically, at $P_S = 25$ dBm, the SEPs of the SISO system are 2.7×10^{-2}, 4×10^{-3}, and 10^{-3} corresponding to $m = 1, 2$, and 3. In other words, the SEP of the SISO system in the case of $P_S = 25$ dBm reduces 7 times and 4 times when m increases from 1 to 2 and from 2 to 3, respectively. For the cooperative RIS-D system, the SEP curve characteristics are similar to those of the SISO system. However, the differences between SEPs in the cases that $m = 1, 2$, and 3 are remarkable even in low transmission power regime, i.e., $P_S < 15$ dBm. In particular, at $P_S = 10$ dBm, the SEPs of the cooperative RIS-D system are 5.7×10^{-3}, 1.4×10^{-3}, and 7.3×10^{-4} corresponding to $m = 1, 2$, and 3. As the results, although using low transmission power, i.e, $P_S = 10$ dBm, when m increases from 1 to 2 and from 2 to 3, the SEP of the cooperative RIS-D system reduce 4 times and 2 times, respectively. These results again confirm the benefits of the using RISs and cooperative communications for improving the performance of wireless systems.

V. CONCLUSION

In this paper, we exploited the advantages of the cooperative communications and the RISs by combining them in a wireless communication system. Specifically, we mathematically analyzed the performance of the cooperative RIS-D system where the multiple reflecting links created by multiple RISs are combined with the direct link between source and destination. We successfully derived the SEP expression of the considered cooperative RIS-D system over Nakagami-m fading channels. Then, the obtained expression was used to consider the impacts of the system parameters. Numerical results clearly shown that the SEP of the cooperative RIS-D system is significantly lower than that of the SISO system. In particular, to achieve a certain SEP target, the transmission power of the cooperative RIS-D system is greatly lower than that of the SISO system. Also, for a certain transmission power, the performance of the cooperative RIS-D system is significantly higher than that of the SISO system. Therefore, exploiting multiple RISs and cooperative communications can greatly save the energy consumption and significantly improve the performance of the cooperative RIS-D system in comparison with the SISO system. We also observed that the RISs located near the source can reflect signals better than the case that the RISs located near the destination. On the other hand, the impacts of various system parameters such as the number of REs in each RIS, number of RISs, and the Nakagami-m parameter were fully investigated to consider their influences on the SEP of the cooperative RIS-D system.

REFERENCES

[1] P. Yang, Y. Xiao, M. Xiao, and S. Li, "6G Wireless communications: Vision and potential techniques," *IEEE Netw.*, vol. 33, no. 4, pp. 70–75, Jul./Aug. 2019.

[2] D.-T. Do, A.-T. Le, N.-D.-X. Ha, and N.-N. Dao, "Physical layer security for Internet of Things via reconfigurable intelligent surface," *Future Gener. Comput. Syst.*, vol. 126, pp. 330–339, Jan. 2022.

[3] S. Atapattu, R. Fan, P. Dharmawansa, G. Wang, J. Evans, and T. A. Tsiftsis, "Reconfigurable intelligent surface assisted two-way communications: Performance analysis and optimization," *IEEE Trans. Commun.*, vol. 68, no. 10, pp. 6552–6567, Oct. 2020.

[4] T. Hou, Y. Liu, Z. Song, X. Sun, and Y. Chen, "MIMO-NOMA networks relying on reconfigurable intelligent surface: A signal cancellation-based design," *IEEE Trans. Commun.*, vol. 68, no. 11, pp. 6932–6944, Nov. 2020.

[5] A.-A. A. Boulogeorgos and A. Alexiou, "Performance analysis of reconfigurable intelligent surface-assisted wireless systems and comparison with relaying," *IEEE Access*, vol. 8, pp. 94463–94483, 2020.

[6] B. C. Nguyen, T. M. Hoang, L. T. Dung, and T. Kim, "On performance of two-way full-duplex communication system with reconfigurable intelligent surface," *IEEE Access*, vol. 9, pp. 81274–81285, 2021.

[7] E. Björnson, O. Özdogan, and E. G. Larsson, "Intelligent reflecting surface versus decode-and-forward: How large surfaces are needed to beat relaying?" *IEEE Wireless Commun. Lett.*, vol. 9, no. 2, pp. 244–248, Feb. 2020.

[8] E. Basar, M. D. Renzo, J. De Rosny, M. Debbah, M. Alouini, and R. Zhang, "Wireless communications through reconfigurable intelligent surfaces," *IEEE Access*, vol. 7, pp. 116753–116773, 2019.

[9] I. Yildirim, A. Uyrus, and E. Basar, "Modeling and analysis of reconfigurable intelligent surfaces for indoor and outdoor applications in future wireless networks," *IEEE Trans. Commun.*, vol. 69, no. 2, pp. 1290–1301, Feb. 2021.

[10] K. O. Odeyemi, P. A. Owolawi, and O. O. Olakanmi, "Reconfigurable intelligent surface assisted mobile network with randomly moving user over Fisher–Snedecor fading channel," *Phys. Commun.*, vol. 43, Dec. 2020, Art. no. 101186.

[11] Y. Chen, B. Ai, H. Zhang, Y. Niu, L. Song, Z. Han, and H. V. Poor, "Reconfigurable intelligent surface assisted device-to-device communications," *IEEE Trans. Wireless Commun.*, vol. 20, no. 5, pp. 2792–2804, May 2021.

[12] A. Hemanth, K. Umamaheswari, A. C. Pogaku, D.-T. Do, and B. M. Lee, "Outage performance analysis of reconfigurable intelligent surfaces-aided NOMA under presence of hardware impairment," *IEEE Access*, vol. 8, pp. 212156–212165, 2020.

[13] T. N. Do, G. Kaddoum, T. L. Nguyen, D. B. da Costa, and Z. J. Haas, "Multi-RIS-aided wireless systems: Statistical characterization and performance analysis," *IEEE Trans. Commun.*, vol. 69, no. 12, pp. 8641–8658, Dec. 2021.

[14] A. Bansal, K. Singh, and C.-P. Li, "Analysis of hierarchical rate splitting for intelligent reflecting surfaces-aided downlink multiuser MISO communications," *IEEE Open J. Commun. Soc.*, vol. 2, pp. 785–798, 2021.

[15] M. D. Renzo, K. Ntontin, J. Song, F. H. Danufane, X. Qian, F. Lazarakis, J. de Rosny, D. Phan-Huy, O. Simeone, R. Zhang, M. Debbah, G. Lerosey, M. Fink, S. A. Tretyakov, and S. Shamai (Shitz), "Reconfigurable intelligent surfaces vs. relaying: Differences, similarities, and performance comparison," *IEEE Open J. Commun. Soc.*, vol. 1, pp. 798–807, 2020.

[16] J. D. V. Sanchez, L. Urquiza-Aguiar, M. C. P. Paredes, and F. J. Lopez-Martinez, "Expectation-maximization learning for wireless channel modeling of reconfigurable intelligent surfaces," *IEEE Wireless Commun. Lett.*, vol. 10, no. 9, pp. 2051–2055, Sep. 2021.

[17] L. Yang, Y. Yang, D. B. D. Costa, and I. Trigui, "Outage probability and capacity scaling law of multiple RIS-aided networks," *IEEE Wireless Commun. Lett.*, vol. 10, no. 2, pp. 256–260, Feb. 2021.

[18] P. K. Sharma and P. Garg, "Intelligent reflecting surfaces to achieve the full-duplex wireless communication," *IEEE Commun. Lett.*, vol. 25, no. 2, pp. 622–626, Feb. 2021.

[19] A. M. Salhab and M. H. Samuh, "Accurate performance analysis of reconfigurable intelligent surfaces over rician fading channels," *IEEE Wireless Commun. Lett.*, vol. 10, no. 5, pp. 1051–1055, May 2021.

[20] Q. Guan, F. R. Yu, S. Jiang, and V. C. M. Leung, "Joint topology control and authentication design in mobile ad hoc networks with cooperative communications," *IEEE Trans. Veh. Technol.*, vol. 61, no. 6, pp. 2674–2685, Jul. 2012.

[21] A. A. Amin and S. Y. Shin, "Capacity analysis of cooperative NOMA-OAM-MIMO based full-duplex relaying for 6G," *IEEE Wireless Commun. Lett.*, vol. 10, no. 7, pp. 1395–1399, Jul. 2021.

[22] Q. Q. Wu and R. Zhang, "Beamforming optimization for wireless network aided by intelligent reflecting surface with discrete phase shifts," *IEEE Trans. Commun.*, vol. 68, no. 3, pp. 1838–1851, May 2020.

[23] H. L. Zhang, B. Y. Di, L. Y. Song, and Z. Han, "Reconfigurable intelligent surfaces assisted communications with limited phase shifts: How many phase shifts are enough?" *IEEE Trans. Veh. Technol.*, vol. 69, no. 4, pp. 4498–4502, Apr. 2020.
[24] V. S. Asadchy, M. Albooyeh, S. N. Tcvetkova, A. Díaz-Rubio, Y. Ra'di, and S. A. Tretyakov, "Perfect control of reflection and refraction using spatially dispersive metasurfaces," *Phys. Rev. B, Condens. Matter*, vol. 94, no. 7, Aug. 2016, Art. no. 075142.
[25] W. Mei and R. Zhang, "Cooperative beam routing for multi-IRS aided communication," *IEEE Wireless Commun. Lett.*, vol. 10, no. 2, pp. 426–430, Feb. 2021.
[26] A. Goldsmith, *Wireless Communications*. Cambridge, U.K.: Cambridge Univ. Press, 2005.
[27] M. Abramowitz and I. A. Stegun, *Handbook of Mathematical Functions With Formulas, Graphs, and Mathematical Tables*, vol. 9. New York, NY, USA: Dover, 1972.
[28] A. Jeffrey and D. Zwillinger, *Table of Integrals, Series, and Products*. New York, NY, USA: Academic, 2007.
[29] D. B. da Costa, H. Ding, and J. Ge, "Interference-limited relaying transmissions in dual-hop cooperative networks over Nakagami-m fading," *IEEE Commun. Lett.*, vol. 15, no. 5, pp. 503–505, May 2011.
[30] D. L. Galappaththige, D. Kudathanthirige, and G. Amarasuriya, "Performance analysis of distributed intelligent reflective surface aided communications," in *Proc. GLOBECOM IEEE Global Commun. Conf.*, Dec. 2020, pp. 1–6.

VAN-DUC PHAN received the M.S. degree from the Department of Electric, Electrical and Telecommunication Engineering, Ho Chi Minh City University of Transport, Ho Chi Minh City, Vietnam, and the Ph.D. degree from the Department of Mechanical and Automation Engineering, Da-Yeh University, Taiwan, in 2016. His research interests include sliding mode control, non-linear systems or active magnetic bearing, energy harvesting enabled cooperative networks, improving the optical properties, lighting performance of white LEDs, energy efficiency LED driver integrated circuits, and novel radio access technologies.

BA CAO NGUYEN received the B.S. degree from Telecommunication University, Khanh Hoa, Vietnam, in 2006, the M.S. degree from the Posts and Telecommunications Institute of Technology (VNPT), Ho Chi Minh City, Vietnam, in 2011, and the Ph.D. degree from Le Quy Don Technical University, Hanoi, Vietnam, in 2020. He is currently working as a Lecturer with Telecommunications University. His research interests include energy harvesting, full-duplex, spatial modulation, NOMA, MIMO, RIS, and cooperative communication.

TRAN MANH HOANG received the B.S. degree in communication command from Telecommunications University, Ministry of Defense, Khanh Hoa, Vietnam, in 2002, the B.Eng. degree in electrical engineering from Le Quy Don Technical University, Hanoi, Vietnam, in 2006, the M.Eng. degree in electronics engineering from the Posts and Telecommunications Institute of Technology, (VNPT), Vietnam, in 2013, and the Ph.D. degree from Le Quy Don Technical University, in 2020. He is currently working as a Lecturer with Telecommunications University. His research interests include energy harvesting, non-orthogonal multiple access, and signal processing for wireless cooperative communications.

TAN N. NGUYEN (Member, IEEE) received the B.S. and M.S. degrees in electronics and telecommunications engineering from the Ho Chi Minh University of Natural Sciences, in 2008 and 2012, respectively, and the Ph.D. degree in computer science, communication technology and applied mathematics from the VSB—Technical University of Ostrava, Czech Republic, where he is currently pursuing the Ph.D. degree in electrical engineering. He joined the Faculty of Electrical and Electronics Engineering, Ton Duc Thang University, Vietnam, in 2013, where he has been working as a Lecturer, since 2013. His major interests are cooperative communications, cognitive radio, physical layer security, and signal processing.

PHUONG T. TRAN (Senior Member, IEEE) was born in Ho Chi Minh City, Vietnam, in 1979. He received the B.Eng. and M.Eng. degrees in electrical engineering from the Ho Chi Minh University of Technology, Ho Chi Minh City, in 2002 and 2005, respectively, the M.S. degree in mathematics, and the Ph.D. degree in electrical and computer engineering from Purdue University, USA, in 2013. In 2007, he became a Vietnam Education Foundation Fellow at Purdue University. In 2013, he joined the Faculty of Electrical and Electronics Engineering, Ton Duc Thang University, Vietnam. He has been working as the Vice Dean of Faculty, since October 2014. His research interests include wireless communications and network information theory.

BUI VU MINH received the degree in electrical and electronic engineering from Nguyen Tat Thanh University, Ho Chi Minh City, Vietnam, in 2015, and the master's degree in electrical engineering from the Ho Chi Minh City University of Technology and Education, Ho Chi Minh City, in 2019. In 2014, he joined the Faculty of Mechanical, Electrical, Electronic & Automotive Engineering, Nguyen Tat Thanh University, and the Laboratory-Practice Management, where, he was a Lecturer, in 2017. His research interests include artificial neural networks and wireless networks.

MIROSLAV VOZNAK (Senior Member, IEEE) received the Ph.D. degree in telecommunications from the Faculty of Electrical Engineering and Computer Science, VSB—Technical University of Ostrava, in 2002, and the Habilitation degree, in 2009. He was appointed as a Full Professor in electronics and communications technologies, in 2017. According to the Stanford University study released, in 2020, he is one of the World's Top 2% of scientists in Networking & Telecommunications and Information & Communications Technologies. He served as the General Chair of the 11^{th} IFIP Wireless and Mobile Networking Conference, in 2018, and the 24^{th} IEEE/ACM International Symposium on Distributed Simulation and Real Time Applications, in 2020. He participated in six projects funded by EU in programs managed directly by European Commission. He is currently a Principal Investigator in the Research Project QUANTUM5 funded by NATO, which focuses on the application of quantum cryptography in 5G campus networks. He has authored and coauthored over 100 articles indexed in SCI/SCIE journals. His research interests include ICT, especially on quality of service and experience, network security, wireless networks, and big data analytics.